Problems associated with direct displacement-based design of concrete bridges with single-column piers, and some suggested improvements

A.J. Kappos,[1] I. Gidaris,[1] K.I. Gkatzogias[1]

Abstract. Currently available displacement-based design (DBD) procedures for bridges are critically evaluated with a view to identifying extensions and/or modifications of the procedure, for it to be applicable to final design of a fairly broad class of bridges. An improved direct DBD procedure is presented, including a suite of comprehensive design criteria and proper consideration of the degree of fixity of the pier top. The design of an overpass bridge (originally designed to a current European Code), applying the improved DDBD procedure is presented and both 'conventional' and displacement-based designs are assessed using non-linear response-history analysis (NLRHA); comparisons are made in terms of both economy and seismic performance of the different designs. It is seen that DDBD provided a more rational base shear distribution among piers and abutments when compared to the force-based design (FBD) procedure and adequately captured the displacement pattern, closely matching the results of the more rigorous NLRHA.

Keywords displacement-based design; bridges; reinforced concrete; Eurocode 8

1 Introduction

Although displacement-based design (DBD) procedures are now well-established for buildings (Kappos 2010), application of these concepts to bridges has been more limited, despite the fact that publications regarding the so-called 'direct' displacement-based design (DDBD) of bridge piers (Kowalsky et al. 1995) or even entire bridges (Calvi & Kingsley 1995) appeared in the mid-1990s. A key reason for this more limited application of DDBD to bridges is the important role that higher modes play in the transverse response of bridges, even of some relatively short ones (Paraskeva & Kappos 2010), which complicates the proper assessment of the displaced shape of the bridge and the target displacement. It is noted that for systems such as multi-span bridges, the DDBD approach requires that the engineer define a target displacement profile (duly accounting

[1] Aristotle University of Thessaloniki, Civil Engineering Department, Laboratory of Reinforced Concrete & Masonry Structures, 54124, Greece, phone: +302310995743, fax: +302310995614, email: ajkap@civil.auth.gr

for inelastic response), rather than just a single target displacement (as in the case of single-column bridges); this usually requires a number of iterations, which inevitably increases the complexity of the procedure.

A DDBD procedure applicable to a fairly broad range of continuous bridge typologies was proposed by Kowalsky in 2002, and further developed by Dwairi & Kowalsky (2006); a key feature of the method was the EMS (effective mode shape) approach wherein account is taken of higher mode effects by determining the mode shapes of an equivalent elastic model of the bridge based on the column and abutment secant stiffness values at maximum response. A similar version of the method was included in the book by Priestley et al. (2007) on DDBD; this version of the method is simpler than the previously mentioned one (no use of EMS in the design of piers) but also addresses design in the longitudinal direction (which often governs), and provides some guidance for the treatment of features like the degree of fixity of columns and the effect of higher modes on the superstructure (the deck) through an EMS approach focusing on forces and moments of the deck only. A contribution to the 'indirect' displacement-based design of bridges was made by Bardakis & Fardis (2008), who extended to bridges the concept of calculating inelastic rotation demands from elastic analysis previously used for buildings by Fardis and co-workers. More recently, Adhikari et al. (2010), focussed on the difficulties involved in applying DDBD to long-span bridges with tall piers. Finally, the DDBD method was improved by Suarez and Kowalsky (2010) by introducing specific guidance for approximating P-Δ effects in defining the target displacement, accounting for skewness effects, and treating bridges with expansion joints within the deck as a whole, rather than as isolated segments extending from joint to joint.

The motivation of the present study was to make the attractive concept of DDBD more suitable for the *final* design of a sufficiently broad class of bridges, so that it can be deemed suitable for practical application. It is worth recalling here that, as correctly pointed out in one of the first papers on DDBD (Calvi & Kingsley 1995), the concept of the equivalent elastic structure (based on member secant stiffness at target displacement) is feasible and preferable in the preliminary design of the bridge, whereas more sophisticated tools (like nonlinear analysis) are recommended at the final design stage. As will be discussed in more detail in the next section, the currently available DDBD procedures work well for the preliminary design of first-mode-dominated bridges in high seismic hazard areas, but present problems in several cases that are common in practice, like bridges with some degree of irregularity, while they are simply not

applicable in low and moderate seismic hazard regions. It is emphasised that the present study does not claim to provide a comprehensive solution to all problems involved; it is rather a contribution in this direction, and addresses only some of the problems identified in the next section.

For the DDBD method to be applicable to the design for transverse response of bridges with some degree of irregularity, higher mode effects have to be treated as part of the entire design procedure (rather than as a correction of deck shears and moments at the final steps). Hence, in the DDBD method proposed in the present study the EMS technique (Kowalsky 2002), is included as part of the procedure. In the comprehensive study by Dwairi & Kowalsky (2006) a number of idealized bridge configurations were analyzed and the results were used for developing guidelines for the selection of displacement patterns (normalized deformed shapes) for continuous bridges with 'rigid translation' and 'flexible symmetric' deformation patterns. These are useful concepts for preliminary design of bridges, but most actual bridges do not fully comply with these idealizations, e.g. the assumption that all columns have the same longitudinal steel ratio and column diameter, or the assumption that piers are hinged to the soffit of the deck, do not hold for most actual bridges. A procedure is then needed that recognises the fact that design codes require taking into account all the peculiarities of each (real) bridge. It is worth noting here that currently DDBD is not adopted by any existing national code as a stand-alone design method. Design documents that are based on the displacement-based concept, such as the recent AASHTO (2009) Guidelines, require (among other things) the use of nonlinear analysis procedures as part of the design; this inevitably introduces complexity and increases the design effort, especially since the advanced analysis tools have to be used in a number of iterations if over-conservatism is to be avoided. Hence, the initial stimulus for the present study was exactly this point, i.e. to identify required extensions and/or modifications of the aforementioned DBD procedure, for it to be applicable to actual bridges wherein the simplifying assumptions made at various stages of the procedure (see next section) do not really hold. A further objective was to obtain some preliminary quantitative data regarding the advantages (or otherwise) of applying the DDBD method, compared to 'main-stream' force-based design (FBD), adopted by all current codes.

The method was applied to a number of simple, but realistic, bridges, namely typical overpass structures with different configurations. A number of problems were identified while attempting

to apply the aforementioned DBD procedure for redesigning these existing structures and extensions/improvements were introduced in the method, as described in section 2.2. A detailed case-study of the design of an overpass bridge (originally designed to a current European Code), applying the improved DBD procedure is presented in detail, and both the 'conventional' and the displacement-based design are assessed using inelastic response-history analysis for suites of both natural and artificially generated ground motions. Comparisons are made in terms of both economy (reinforcement requirements) and seismic performance of the different designs.

2 Limitations of the existing direct DBD method for bridges and proposed extensions

2.1 Limitations of the existing direct DBD procedure

The DDBD method aims at designing a bridge to achieve a prescribed limit state that may be defined directly from displacements (or drifts), or derived from strain criteria under the selected design earthquake. The procedure utilizes the elastic displacement spectra reduced for an equivalent damping value, and the secant stiffness at the selected design displacement. Hence the stiffness of the bridge is not fixed at the beginning of the procedure (as in FBD) but is derived in the process through the effective period (secant value). This is achieved by reducing the multi-degree of freedom (MDOF) structure to an equivalent single degree of freedom (SDOF) based on the substitute structure concept (Shibata and Sozen 1976). The equivalent SDOF inelastic response is represented by the secant stiffness at peak response and equivalent damping.

The crucial assumption involved in the above procedure is that this SDOF system suffices for capturing the displacements of the bridge (whose response is typically inelastic, for all limit states beyond that corresponding to full serviceability); this implies that a single mode (which might, in fact, be a fictitious one, see subsequent sections) is used for deriving the properties of the equivalent SDOF system. The idea of the 'effective mode shape' (EMS) proposed by Kowalsky (2002), building on concepts previously put forward by Calvi & Kingsley (1995), is a useful one in this respect; it involves the estimation of a fictitious mode shape of the (inelastically responding) bridge by a statistical combination of individual modes. It is important to note that these modes are also fictitious ones, since they are not the (elastic) normal modes of the bridge but they are derived by eigenvalue analysis of a bridge model wherein yielding members (such as piers and, wherever applicable, abutments) are modelled with their secant stiffness at the intended

displacement (that generally exceeds the yield displacement, hence inelastic response is foreseen). It is clear from the foregoing summary of the procedure that, in general, a substantial number of iterations would be required to define effective mode shapes consistent with the inelastic response of the bridge to the design earthquake, even more so when multiple earthquake intensities are considered for checking multiple limit states (performance requirements). This important limitation of the method has been remedied to a certain extent by the 'calibration' of inelastic displacement patterns carried out by Dwairi & Kowalsky (2006) who performed response-history analyses of four-span bridges with regular and irregular pier configurations, and with different support conditions at the abutments, for a set of 12 recorded motions.

To simplify things and improve convergence of the procedure, existing DDBD methods typically assume that the transverse response of single-column piers, even those monolithically connected to the superstructure, is that of a simple cantilever. Priestley et al. (2007) note that "it is important to correctly model the expected moment pattern in the piers during the design process", but they do not include the determination of the degree of fixity at the pier's top as part of the design procedure that they propose for the transverse direction. Consideration of the pier as a simple cantilever, which implies that the superstructure has zero or negligible torsional stiffness, or, in the case of bearing-supported decks, a single central bearing is used in each pier, results to significant increase in the required steel ratio at the base of the pier. In the common case of a box girder deck, the assumption of negligible torsional stiffness can be realistic only in the case of yielding of the superstructure's transverse reinforcement (Katsaras et al. 2009). However, this situation is not permitted by current seismic codes, wherein the superstructure is required to remain (essentially) elastic under the design earthquake. Moreover, proper consideration of the expected moment pattern in the piers has a significant importance in the case of the DDBD procedure, as it affects the yield displacement (hence the displacement ductility demand) and the flexural stiffness of the piers. It is also noted here that when the deck is massive and of large width (not the case in overpass bridges studied herein), the mass moment of inertia of the deck can result in non-negligible moments (of either sign) at the deck's mass centre. The corresponding rotational dynamic degree of freedom cannot be included in the DDBD procedure that is based on an equivalent static approach; Priestley et al. (2007) recommend that the effect of the associated higher modes be accounted for in the capacity design of piers for shear (through a dynamic amplification factor ω).

A more general limitation of all DDBD procedures is the fact that not all bridges are, or should be made, displacement-controlled. There are two typical 'scenarios' wherein DDBD is not meaningful:

First, the case of regions of low, moderate, and even moderate-to-high seismic hazard, where the maximum displacement defined by the pertinent design spectrum is too low, even when no additional viscous damping (accounting for inelastic response) is introduced. Just as an example, seismic Zone I in Greece (which is the country with the highest seismicity in the European Union) is characterized by a design PGA=0.16g and a design spectrum, according to Eurocode 8 (CEN, 2005) for the common case of ground C, that results in a maximum elastic displacement (for 5% damping) of only 119 mm at a period T_D=2.0 sec (the Eurocode 8 recommended value for the threshold of the constant displacement branch of the spectrum). This is lower than the pier yield displacement, even in a bridge with relatively short piers like the overpass reported in detail in Section 5 and App. A of the paper. In fact, to make DDBD meaningful to the common bridge configurations studied by the authors, higher seismic hazard (Zones II and III) and more conservative assumptions (T_D=4.0 sec) for the displacement spectrum had to be used. For bridges with (relatively) tall piers even these conservative assumptions cannot lead to meaningful DDBD. It is worth adding here that there is no guarantee that for reinforced concrete (R/C) piers that are not displacement-controlled, reinforcement provided for satisfying vertical loading requirements will also be sufficient for earthquake resistance.

Second, the configuration of the bridge, including support conditions, which must also account for soil-structure interaction (SSI), should be such as to permit substantial displacements, accompanied by inelastic action. The case of bridges with tall piers has been mentioned previously, another case is that of bridges with transverse displacement blocked at the abutments. For instance, in the bridge reported in section 5, which is a typical overpass structure, blocking of transverse movement through stoppers at the (seat-type) abutments leads to very small displacements of the piers subsequent to their yielding, as most of the base shear developed after that stage goes to the abutments. It is worth noting here that design methods for integral bridges aiming at the minimization of displacements have recently been proposed; in fact some researchers (Mitoulis & Tegos 2010) have suggested the addition of external restraining systems (consisting of IPE-steel piles) as means of retrofitting of existing bridges by limiting their seismic

displacements. In all these bridge configurations application of the existing DDBD methods is simply not meaningful.

Last and not least, for DDBD procedures for bridges to be suitable for practical design, they should be enriched with additional design criteria that would avoid the situation (that the authors have encountered on several occasions in their case-studies) wherein the advantages of DBD (with respect to FBD) are lost when minimum requirements for dimensioning and detailing of reinforced concrete (R/C) members are applied, in line with current practice. Therefore, additional criteria have to be introduced at the early steps of the DDBD procedure.

The extensions to the DDBD method proposed in the next section aim at remedying some of the aforementioned limitations. Other critical issues (currently being studied by the authors) like the effect of higher modes and the presence of tall piers will be addressed in a future publication; a pilot version of the methodology suggested for properly accounting for higher mode effects can be found in Kappos et al. (2011).

2.2 Proposed extensions to the existing procedure

Various design criteria (complementary to those already included in the DDBD procedure) are proposed herein; they constitute guidelines that can assist the practicing engineer to achieve an efficient design, regarding both performance and economy. An extension of the DDBD procedure, mainly intended for bridges with single-column piers monolithically connected to the superstructure, is then proposed, wherein the degree of fixity to pier top provided by superstructure torsional stiffness is taken into consideration. Extension of the procedure to the case of multi-column bents (acting in their transverse direction) is relatively straightforward, but is not addressed herein. It should be noted that in multi-column bents the effect of the common approximation is the opposite of that in single-column piers, i.e. assuming the contraflexure point to be at column midheight (which is generally a more reasonable assumption than assuming cantilever action of single columns) underestimates the moment that can actually develop at either end of the column.

A pragmatic design approach is to meet as many criteria as possible with the least number of iterations. The additional design criteria proposed herein as an integral part of the DDBD method are as follows:

i. $\boldsymbol{V_{abt} \leq V_u}$**:** The shear carried by each abutment (V_{abt}) should not exceed the ultimate shear (V_u), which is directly related to the 'weakest link' of the superstructure-abutment-backfill (SAB) system. For instance, in the case of a bearing-supported superstructure (with or without seismic links), it can be assumed that the SAB system will respond quasi-elastically ($K_{SAB} = K_{Bearings}$) until the closure of the gap between the deck and the abutment or seismic link; thus, V_u can be calculated from the ultimate force that can develop in the elastomeric bearings placed at the abutment, or the resistance of the seismic link. Activation of the abutment-backfill system can in turn determine V_u; this is also the 'weakest link' in the case of a monolithic superstructure-abutment connection.

ii. $\boldsymbol{V_{pier} \geq V(\rho_{req}=\rho_{min})}$**:** The shear carried by each pier (V_{pier}) should exceed, for the sake of economical design the shear (and hence the moment) that corresponds to the minimum required longitudinal reinforcement ratio, $V(\rho_{req}=\rho_{min})$. Otherwise, code minimum requirements will prevail and any benefits of DBD will probably vanish.

iii. $\boldsymbol{k_{eff} \geq k(T_{eff}=T_D)}$**:** Calculated supporting member (pier/abutment) secant stiffnesses, (corresponding to the target-displacement profile), and hence the secant stiffness (k_{eff}) of the equivalent SDOF system (see Step 4 in section 3) should not correspond to an effective period (T_{eff}) longer than the threshold (T_D) of the constant displacement branch of the design spectrum (see §3 and Figures 2, 6). As also noted by Priestley et al. (2007), when $T_{eff} > T_D$ no unique design solution can be found. It is recognised, though, that in structures with tall piers (not addressed herein) the maximum elastic displacement (corresponding to $T \geq T_D$) could be less than the yield displacement. In such cases 'standard' DDBD is not applicable, and other requirements such as P-Δ effects (see also point iv) or gravity and/or wind load combinations will determine the pier strength.

iv. $\boldsymbol{\mu_{pier} \leq \mu_d}$**:** In 'standard' DDBD, pier target-displacements should not exceed the corresponding limit-state displacement capacities (Δ_d), determined either from strain-based criteria (Kowalsky 2000) or drift-based criteria ($\Delta_{pier} \leq \Delta_d$). P-Δ effects should also be considered (see §3, Step 14). If drift criteria (which are easier to apply) are used, an allowable displacement ductility value (μ_d), determined by the designer (taking into account the detailing rules used in dissipating zones), should be introduced in the design as an explicit check for the piers.

v. $\Delta_{abt} \leq \Delta_d$: As in design criterion (i), the abutment target-displacements should not exceed the corresponding limit-state displacements capacities (Δ_d), defined in accordance with the SAB system configuration. Referring to the common case of a bearing-supported (at the abutments) superstructure, Δ_d is calculated in terms of the maximum acceptable shear strain ratio (γ_u), given the bearing horizontal stiffness; it is noted that in the design in the longitudinal direction the bearing strains should include the contribution of displacements due to dead loads, creep and shrinkage, and temperature variations.

An ideal design solution would meet all the above design criteria as equations (=) instead of inequalities ($\leq$ or $\geq$); clearly, such a solution is not feasible in practical design.

In the extension of the existing DDBD method presented herein, the parameter of the equivalent cantilever length (H_0), which is the distance from the pier base to the contraflexure point (see Figure 1), is introduced to take into account the degree of fixity at the top of the pier. The yield displacement of the pier and the flexural stiffness for the transverse response can be determined based on an equivalent cantilever with height equal to H_0. The yield displacement ($\Delta_{y,pier}$) and the flexural stiffness (K_{pier}) of each pier are given by Equations 1 and 5, respectively. In Equation 1, $\Delta_{y,eq}$ is the yield displacement of the equivalent cantilever and n is the ratio of H_0 to the pier total height H. $\Delta_{y,eq}$ can be calculated from Equation 2 where the yield curvature φ_y can be estimated from the empirical Equation 3 (Priestley et al. 2007), wherein ε_y is the reinforcement yield strain and D the circular section diameter; other column sections can also be addressed in a similar fashion. Substituting Eq. 2 into Eq. 1, results in Equation 4 for $\Delta_{y,pier}$. In Equation 5, K_{eq} is the flexural stiffness of the equivalent cantilever expressed as in Equation 6, where E is the elastic modulus of concrete and I is the moment of inertia of the pier cross-section (modified for cracking effects wherever necessary). Substituting Eq. 6 into Eq. 5, results in Equation 7.

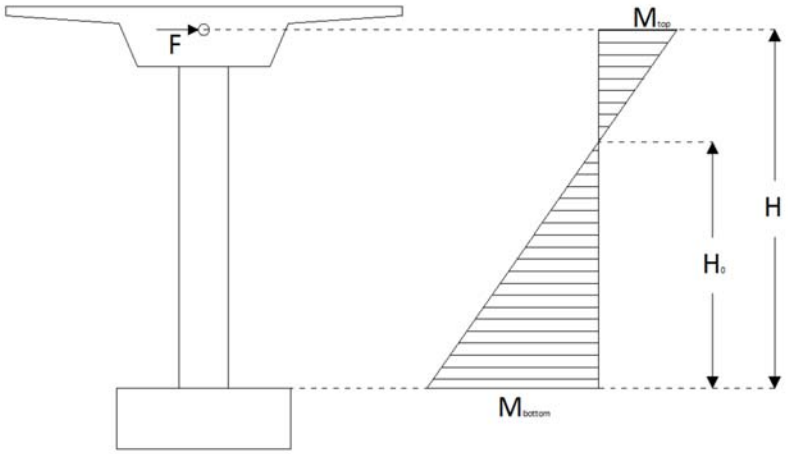

Figure 1. Definition of equivalent cantilever length of a pier under transverse seismic excitation

$$\Delta_{y,pier} = (1/n)\,\Delta_{y,eq} \tag{1}$$

$$\Delta_{y,eq} = \varphi_y \cdot H_o^2/3 = \varphi_y (n \cdot H)^2/3 \tag{2}$$

$$\varphi_y = 2.25(\varepsilon_y/D) \tag{3}$$

$$\Delta_{y,pier} = n(\varphi_y \cdot H^2/3) \tag{4}$$

$$K_{pier} = n \cdot K_{eq} \tag{5}$$

$$K_{eq} = 3 \cdot E \cdot I/H_o^3 = 3 \cdot E \cdot I/(n \cdot H)^3 \tag{6}$$

$$K_{pier} = (1/n^2)(3 \cdot E \cdot I/H^3) \tag{7}$$

3 Step-by- step description of the proposed DDBD procedure

For the sake of completeness, all steps of the procedure for design in the transverse direction of the bridge that presents more challenges than the longitudinal one, including those that are the same as in the existing procedures (Dwairi & Kowalsky 2006, Priestley et al. 2007) are summarised in the following. It is noted that prior to applying the successive steps of the design process, some initial input parameters have to be defined.

Definition of initial input parameters: First, the equivalent cantilever length H_0 (Figure 1) has to be defined. However, this parameter is unknown at the outset of the process, since it

depends on the cracked torsional stiffness of the bridge superstructure, the type of superstructure-abutment connection, and the pier-superstructure relative stiffness. Therefore, as an initial estimate, it is assumed that H_0 is equal to the total height of the pier. This initial value will be revised later, as will be described subsequently. Having defined the equivalent cantilever length, the pier yield displacement (Δ_y) is calculated from Equation 4. Furthermore, limit-state displacement capacities (Δ_d) and allowable displacement ductilities (μ_d) of piers and abutments should be determined according to the design criteria (iv) and (v) in the previous section.

Step 1 - Estimation of the displacement pattern of the bridge: It is noted that the term 'displacement *pattern*' refers to the deformed shape of the bridge deck under transverse seismic excitation, while the term 'displacement *profile*' refers to the numerical values of the displacements of the deck. In the general case, where the flexibility of the deck has to be taken into account, the displacement pattern is obtained using the effective mode shape (EMS) method proposed by Kowalsky (2002). For regular bridges whose thansverse response is dominated by one mode only, approximate patterns proposed in the relevant literature (e.g. Dwairi & Kowalsky 2006) could be used, especially at the preliminary design stage.

The EMS method is iterative in nature and consists of the following steps:

i. **Evaluate mode shapes (φ_j)**: At the start of the process member properties are unknown, therefore an initial estimate is required. It is commonly assumed that a prestressed concrete superstructure will respond essentially elastically (e.g. CEN, 2005) in flexure, hence uncracked flexural rigidity can be considered in analysis, while torsional cracking of the deck can be assumed and the corresponding stiffness could be set equal to 10÷30% of the uncracked stiffness (Katsaras et al. 2009). In the common case where piers are expected to respond inelastically, it is necessary to consider effective properties. The DDBD approach adopts secant stiffness to maximum response, thus it is suggested that a secant stiffness equal to 10% of the uncracked section stiffness be applied, while a stiffness equal to 60% of the uncracked section stiffness is suggested for columns that are expected to remain elastic. Once the structure properties have been established, the eigenvalue problem and hence the mode shapes can be obtained. As noted earlier, the so-derived modes are not the natural modes of the elastic structure, but rather fictitious ones, based on effective properties of an inelastically responding structure.

ii. **Evaluate modal participation factors (Γ_j):** The modal participation factors can be calculated as given in Equation 8, where $\boldsymbol{M}$ represents a diagonal mass matrix and $\boldsymbol{\iota}$ is a unit vector.

$$\Gamma_j = \left(\boldsymbol{\varphi}_j^T \cdot \boldsymbol{M} \cdot \boldsymbol{\iota}\right) \Big/ \left(\boldsymbol{\varphi}_j^T \cdot \boldsymbol{M} \cdot \boldsymbol{\varphi}_j\right) \tag{8}$$

iii. **Evaluate modal displacements ($\delta_{i,j}$):** Compute the expected modal displacement of each bent according to Equation 9 where index i represents the bent number, index j represents the mode number, hence $\varphi_{i,j}$ is the modal factor of bent i and mode j, and $S_{d,j}$ is the spectral displacement for mode j obtained by entering the 5%-damped design spectra with the period obtained from the modal analysis.

$$\delta_{i,j} = \varphi_{i,j} \cdot P_j \cdot S_{d,j} \tag{9}$$

iv. **Evaluate expected displacement pattern (δ_i):** The displacement pattern is obtained by any appropriate combination of the modal displacements, such as square root of the sum of the squares (SRSS) as given by Equation 10 or complete quadratic combination (CQC).

$$\delta_i = \sqrt{\sum_j \delta_{i,j}^2} \tag{10}$$

Step 2 - Estimation of the fraction of the total seismic force carried by the abutments: At this stage of the design the exact fraction (x) of total lateral inertia force carried back to the abutments by superstructure bending is unknown; thus an initial assumption should be made. This is one of the weakest points of the procedure, as, depending on a number of factors (especially the support conditions at the abutment, and also the stiffness of the deck in the transverse direction), x can vary within broad limits; Kowalsky (2002) recommends an initial value x=0.3, Priestley et al. (2007) recommend x=0.4.

Step 3 - Definition of the critical target-displacement profile: Utilizing the limit-state displacement capacities determined at the initial stage, the critical target-displacement profile can be obtained, by scaling (see Equation 11) the displacement pattern to the displacement capacities of each bent; the critical target-displacement profile (Δ_i) is identified as the one where the displacement capacities are not exceeded. In Equation 11 $\Delta_{d,c}$ and δ_c are the displacement capacity and the value of the displacement pattern of the critical bent, respectively.

$$\Delta_i = \delta_i \cdot \Delta_{d,c} \big/ \delta_c \tag{11}$$

Step 4 - Determination of the equivalent SDOF system: In this step an equivalent SDOF system, represented by a system displacement (Equation 12) and a system mass (Equation 13), is established by equating the work done by the MDOF bridge and the corresponding SDOF system (Calvi & Kingsley 1995). In Equations 12 and 13 m_i is the mass associated with bent i and n the number of bents.

$$\Delta_{sys} = \sum_{i=1}^{n}\left(m_i \cdot \Delta_i^2\right) \Big/ \sum_{i=1}^{n}\left(m_i \cdot \Delta_i\right) \tag{12}$$

$$M_{sys} = \left(1/\Delta_{sys}\right)\sum_{i=1}^{n}\left(m_i \cdot \Delta_i\right) \tag{13}$$

Step 5 - Determination of the pier displacement ductilities and equivalent viscous damping ratios: Utilizing the chosen target-displacement profile and estimated yield displacements, the displacement ductility ($\mu_{\Delta,i}$) of each pier is calculated and compared with μ_u, (see design criterion iv). If any $\mu_{\Delta,i}$ exceeds μ_u, the designer should revise either the target-displacement profile (by reducing the pier limit-state displacements) or the yield displacements (e.g. by reducing the pier cross-section). Ideally, this check can be avoided when material strain criteria are used for defining Δ_d at Step 3, but for final design purposes it should be retained given that strain-related target displacements are estimated from relationships (e.g. Kowalsky 2002) that provide average values calculated from parametric analyses of different sections.

Knowing the displacement ductility demand for each pier, the corresponding equivalent viscous damping (in %) is estimated from Equation 14, which is valid for Takeda 'thin' hysteretic rule that generally is suitable for well-confined R/C pier sections (Priestley et al. 2007). Additional elastic viscous damping (ξ_{el}), typically taken as 5% for R/C members, is added to the hysteretic damping.

$$\xi_i = \xi_{el} + 44.4\left(\mu_{\Delta,i} - 1\right)\Big/\left(\pi \cdot \mu_{\Delta,i}\right) \tag{14}$$

Step 6 - Determination of base shear distribution among different bents: Once the individual member damping values are obtained, they must be combined into a value for the equivalent SDOF system. The approach suggested here weighs damping in proportion to the work done by the member (Kowalsky 2002, Priestley et al. 2007). In order to calculate the weighting factors in Equation 15, knowledge of member forces is required. Since shear force distribution is unknown at this stage of the design procedure, it can be assumed that all piers have

equal reinforcement ratio and cross-section. This assumption allows to consider shear forces in piers (V_i) distributed inversely proportionally to the pier heights (H_i), assuming all piers yield and have zero post-yield stiffness and same degree of fixity to the superstructure, as given by Equation 16 (Priestley at al. 2007), where μ is less than one for elastic columns and equal to one for columns that have yielded. The abutment shear forces ($V_{abt,i}$) are distributed according to Equation 17, where $\Delta_{abt,i}$ is the abutment i target displacement. Note that in Equations 16 and 17, V_B is the seismic base shear which is unknown at this stage of the design.

$$Q_i = V_i \cdot \Delta_i \tag{15}$$

$$V_i = V_B (1-x) \frac{\mu_{\Delta,i}}{H_i} \Big/ \sum_{i=1}^{n} \left(\mu_{\Delta,i} / H_i \right) \tag{16}$$

$$V_{abt,i} = V_B \cdot x \cdot \Delta_{abt,i} \Big/ \left(\Delta_{abt,1} + \Delta_{abt,2} \right) \tag{17}$$

Step 7 - Determination of the equivalent system damping: The equivalent system damping (ξ_{sys}) is calculated by combining individual member damping ratios, according to Equation 18 (where the weighting factors Q_i are calculated from Eq. 15). Since both the numerator and the denominator of this fraction are multiplied by the term V_B, the equation can be applied, despite the fact that V_B is unknown at this stage of design.

$$\xi_{sys} = \sum_{i=1}^{n} \left(Q_i \cdot \xi_i \Big/ \sum_{k=1}^{n} Q_k \right) \tag{18}$$

Step 8 - Determination of the effective period, stiffness and design base shear of the equivalent SDOF system: Utilizing the system target displacement (Δ_{sys}), level of system damping (ξ_{sys}) and elastic response spectra for the chosen seismic demand, the effective period (T_{eff}) is determined as shown in Figure 2. Reduction factors for displacement spectra for damping higher than 5% are available in the literature; those of EC8 (CEN 2005) are used herein (see Appendix A).

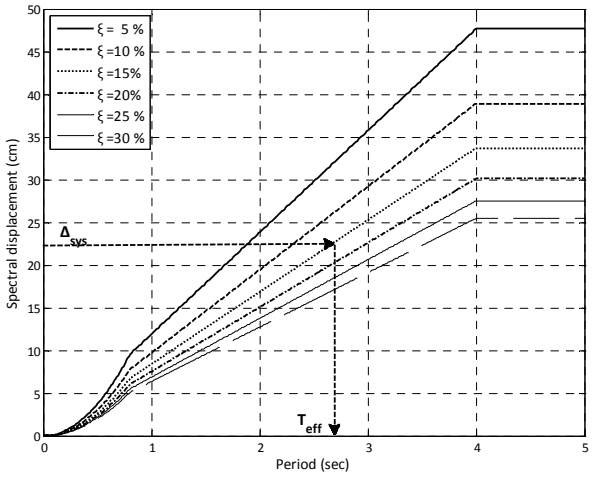

Figure 2. Effective period calculation based on DBD procedure

Once more, revision of the target-displacement profile is required when the calculated Δ_{sys} exceeds the displacement that corresponds to the corner period (T_D) (see design criterion iii). Once the effective period has been determined, effective stiffness (K_{eff}) and design base shear (V_B) are calculated by Equations 19 and 20, respectively.

$$K_{eff} = 4 \cdot \pi^2 \cdot M_{sys} \big/ T_{eff}^2 \tag{19}$$

$$V_B = K_{eff} \cdot \Delta_{sys} \tag{20}$$

Step 9 - Check of effective pier stiffnesses: The design base shear is distributed as discussed in Step 8 (Equations 16 and 17) and the effective stiffness of the piers is calculated using Equation 21. The assumed pier effective stiffness is compared with calculated values; if they differ substantially, Steps 1-9 are repeated, until convergence is achieved.

$$K_{eff,i} = V_i / \Delta_i \tag{21}$$

Step 10 - Distribution of design base shear to inertia mass locations: Once pier effective stiffnesses stabilize, base shear is distributed as inertia forces (F_i) to the masses (m_i) of the MDOF structure in accordance with the target-displacement profile (Δ_i) as given by the equation

$$F_i = V_B \cdot m_i \cdot \Delta_i \Big/ \sum_{i=1}^{n} \left(m_i \cdot \Delta_i \right) \tag{22}$$

Step 11 - Structural analysis: In this step the bridge is analysed using linear static analysis under the inertia loads of Equation 22, in order to obtain the design shear for each pier and abutment. Effective stiffnesses estimated in Step 9 should be used in the structural model analysis, to be consistent with the DDBD philosophy.

Step 12 - Verification of the target displacement profile: The displacement of the critical bent is compared with the selected target-displacement. If the assumed quantities differ significantly from the computed ones, then stiffnesses are changed accordingly, and the analysis is repeated until convergence is achieved and design criteria (i), (iv) and (v) are met.

Step 13 - Verification of equivalent cantilever length: Once the displacement profile obtained from structural analysis converges to the assumed target-displacement profile, column secant stiffnesses and abutment forces from the static analysis are compared with assumed values of Step 9 (at which stabilization of Δ_i was achieved) and Step 2 (at which the seismic force carried by the abutments was taken as a fraction x of the total seismic force carried by the bridge), respectively. In case of significant discrepancy, the target-displacement profile is revised utilizing the EMS method and structural analysis forces. Steps 1-13 are repeated until column secant stiffnesses and abutment forces converge, assuming as a starting point the secant stiffnesses ($k_{eff,i}$), the fraction of the total seismic force carried by the abutments (x) and revised equivalent cantilever lengths ($H_{0,i}$) according to the results of the structural analysis that was previously performed. It is noted that in the case of a superstructure supported on the abutments through bearings the design is simplified since the shear carried by the abutment is known from the first iteration, if the horizontal stiffness of the bearings is assumed constant; therefore iterations are introduced solely due to the updating of the equivalent cantilever lengths.

Step 14 - Verification of P-Δ effects: Stability index (θ_Δ) is calculated according to Equation 23, where P and Δ are the pier axial load and the lateral displacement at the point of contraflexure respectively, while M is the pier base moment, equal to $V \cdot H_0$ (column shear times the equivalent cantilever length). If θ_Δ exceeds 0.10, the design flexural capacity of the pier base should be amplified for P-Δ effects as indicated in Equation 24 (Priestley at al. 2007). For lower values of θ_Δ, P-Δ effects may be ignored, while it is recommended that θ_Δ should not exceed 0.20, otherwise limit-state displacement capacities should be reduced and hence the target-displacement profile should be revised (see design criteria iv and v).

$$\theta_{\Delta} = P \cdot \Delta / M \tag{23}$$

$$M_{design} = M + 0.5 \cdot P \cdot \Delta \tag{24}$$

In cases of slender/tall columns (not specifically addressed herein), where the above check might not be satisfied and might lead to revising the column reinforcement and carrying out additional iterations, it is recommended to adopt the recent proposal of Suarez & Kowaslky (2010) and include as an additional definition of the design displacement (at Step 3) the approximate expression

$$\Delta_{d,c} = 0.85C^{-0.83} \cdot \Delta_y \tag{25}$$

where the empirical coefficient C is estimated from the pier characteristics and axial load, and the peak value of the displacement spectrum (for $T=T_D$).

Step 15 - Design of the MDOF structure: The bridge is designed in accordance with capacity design principles (Priestley at al. 2007) and also design criterion (ii), such that the desired plastic mechanism, as well as economical design are achieved. To meet design criterion (ii) the target-displacement profile and/or the pier cross section might have to be revised and Steps 1 to 15 to be repeated.

4 Example bridge designs

The proposed displacement-based design procedure was applied to an actual bridge structure. The selected Pedini Bridge is an overpass along the Egnatia motorway in Northern Greece. It is a three-span, symmetric bridge, curved in elevation as shown in Figure 3. The deck has a voided T-beam-like prestressed concrete section with a maximum width of 11.0 m and total depth of 1.60 m (see Figure 4); it is supported on two cylindrical piers of 1.70 m diameter and 8.50 m height, which are monolithically connected to the superstructure and the foundation. The deck is resting on each seat-type abutment through two pot bearings that permit sliding along the two principal bridge axes. Transverse displacement at the abutments is blocked (after a 120 mm gap is closed) by a stopper system at the top of the backwall. The pier foundation consists of a 2×2 pile group, connected with a pile cap, while the abutments are supported on a 1×4 pile row; all piles have equal diameter of 1.0 m.

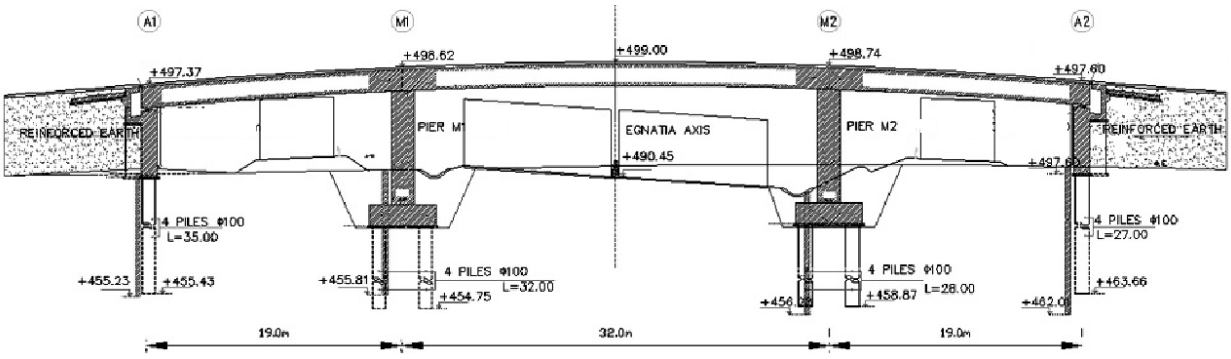

Figure 3. Longitudinal cross-section of the bridge.

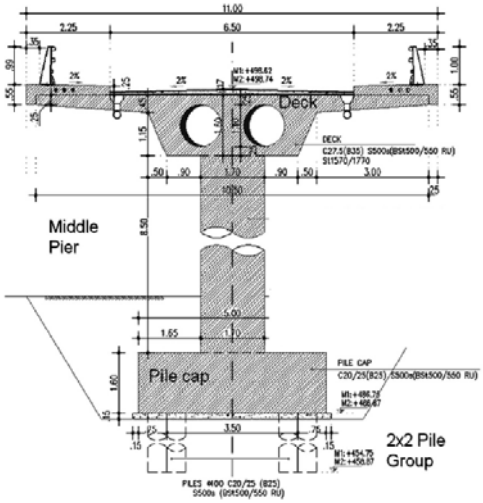

Figure 4. Overview of the foundation-pier-superstructure system cross-section.

The bridge was modelled using the 3D structural analysis program SAP2000 (CSI 2007). A three-dimensional model was set up with beam-column elements to reflect the geometry, boundary conditions, and material behaviour of the bridge studied. As shown in Figure 5, the structure is adequately discretized to account for the bridge parabolic shape in elevation. Details of the modelling of the bridge are given in Kappos & Sextos (2009), where different scenarios of soil-structure interaction are explored; here, the case used for design was that where the single-column piers are fixed at the foundation level.

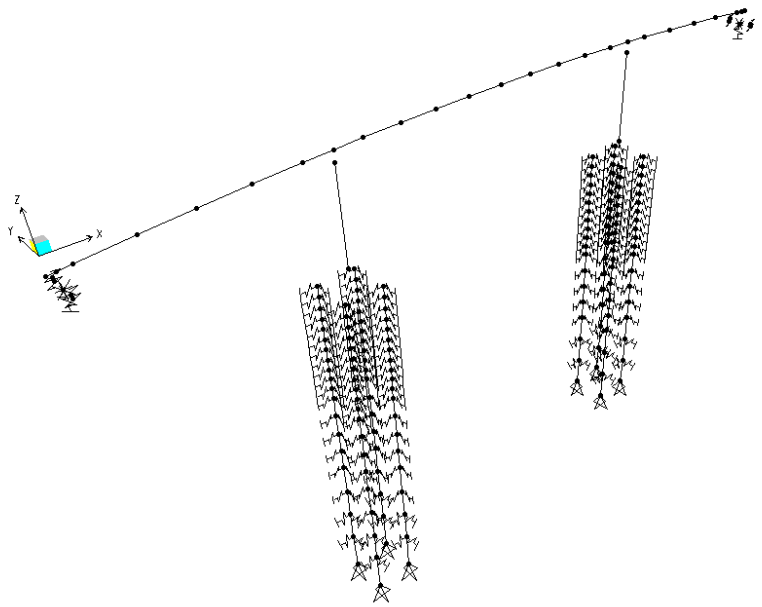

Figure 5. Basic layout of the 3D model that includes the pier foundation.

4.1 Displacement-based design

The DDBD procedure described previously was applied to the selected bridge structure for two different seismic hazard zones, characterised by design ground accelerations a_g=0.24g and a_g=0.36g; these correspond to Zones II and III of the current Greek Seismic Code (EAK 2000), but the corresponding spectra were modified in a number of ways, as described later in this section. It is noted that the actual bridge is located in Zone I (a_g=0.16g) of the Code, but as mentioned earlier DDBD was not meaningful for such low seismic displacements.

For the purposes of this case-study, only the damage control limit state was considered (this is the most commonly adopted criterion for new structures). It was clear from the beginning that for such a bridge configuration, DDBD in the transverse direction would be meaningful only if the stoppers used for blocking the transverse displacement at the abutment were removed (otherwise, transverse displacements would be very small, since, subsequent to pier yielding, most of the seismic base shear is taken by the abutment-backfill system, as shown in Kappos & Sextos, 2009). Hence, the selected support type at the abutments was through elastomeric bearings that can deform unobstructed in either direction (longitudinal-transverse); for this to be feasible the

corresponding gaps between the deck and the stoppers should be equal to at least the pertinent displacement under the design earthquake. The elastomeric bearing geometrical and mechanical characteristics were the result of a first DDBD conducted for the longitudinal direction of the bridge, and then these bearing characteristics were used in the design of the transverse direction. The selected bearings are circular in shape (hence omni-directional) and have a diameter of 400 mm, total thickness of the elastomer 100 mm, shear modulus of 0.8 MPa, effective horizontal stiffness of 1010 kN/m and equivalent viscous damping coefficient equal to 10%. For economy of space, the longitudinal DDBD procedure will not be presented in detail herein; the focus will be on the transverse response wherein most of the challenges of DDBD are encountered.

To compute the limit-state displacement capacities, drift-based criteria were used in the case of pier columns, i.e. the drift ratio at each column should not exceed 3%, while for the abutments the limit state was defined based on a maximum acceptable shear strain γ_u=2.0 for the elastomeric bearings.

The elastic design spectra were those of EAK2000, for a_g=0.24g and a_g=0.36g, for site conditions *C*, as in the actual bridge; these are similar to those of Eurocode 8 (EC8) as well as those of ASCE/SEI 7-05 (ASCE 2006), the difference being that the latter introduce an additional soil factor (for soil *C*, S=1.15 in EC8 and S=1.0÷1.2 in ASCE 7, depending on the peak spectral acceleration), which is not included in the Greek Code (that will soon be replaced by EC8). A critical problem with EC8 spectra, if they are used for DDBD is the value of the 'long-period transition period' T_D, after which displacement remains constant (Figures 2, 6); the recommended value in EC8 is 2.0 sec (2.5 sec is adopted in the National Annex of Greece), which is far shorter than the values adopted in other modern codes, such as ASCE 7 (2006), or guidelines for DBD like those of SEAOC (1999) and AASHTO (2009), and there is currently a feeling in Europe that this value might not be adequate in certain situations. In any case, adopting T_D=2.0 sec was found by the writers to lead to low values of peak displacement, hence rendering DDBD meaningless in several cases, particularly of bridges, which are normally characterised by long periods (especially when realistic values are assumed for flexural rigidities of concrete members). In view of these considerations, DDBD was applied herein adopting a value T_D=4.0 sec; this is the same value as in SEAOC, and equals the minimum value in ASCE 7 that specifies values up to 16 sec (adopting T_D>4 sec would not have affected the results of this case-study). Figure 6 shows

the acceleration and displacement spectra for Zone III, the latter generated for various damping ratios, as required in DDBD (displacement spectra for Zone II were shown in Figure 2).

Initially the pier diameter (1.70 m) of the existing bridge was used. However, the pier longitudinal reinforcement demands for the case of Zone II design were found to be less than the minimum requirement (1%) prescribed in the Greek Code for Seismic Design of Bridges (again, very similar to EC8-Part 2). This revealed the need for redimensioning the pier cross-section (see design criterion ii), and a diameter of 1.30 m was finally selected (which also satisfied gravity load requirements). Hence, a more rational and economical design was achieved, the rationality being related to the possibility of achieving the desired displaced shape of the bridge. It is noted that for the case of Zone III design the initial diameter of 1.70 m was not changed, since the required longitudinal reinforcement was found to be higher than the minimum reinforcement requirements specified by the Code.

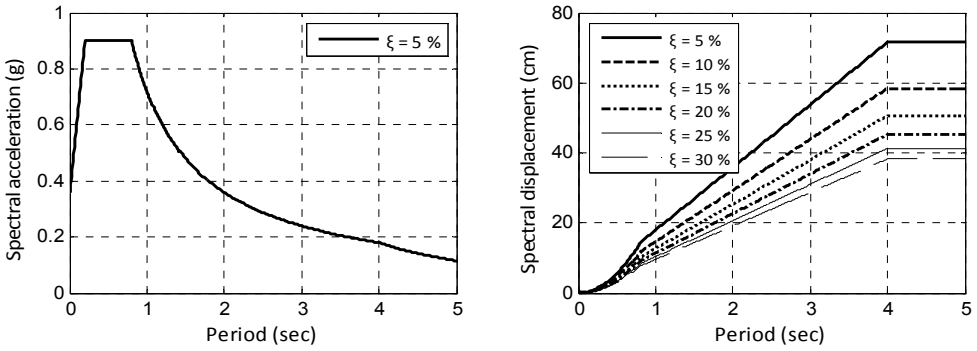

Figure 6. Design response spectra, Soil Type C, Zone III (a_g = 0.36g): acceleration response spectrum (left), and displacement response spectra for various damping ratios (right).

As an example of the application of the procedure, the successive steps for the Zone II design are presented in detail in Appendix I, which also includes a summary table for Zone III design.

4.2 Conventional code design

In addition to applying the DDBD approach, the bridge was also designed for the transverse direction using force-based design, carried out according to the Greek standards (similar to Eurocode 8, as noted earlier). The bridge was designed for two different ground acceleration values, 0.24*g* and 0.36*g* (Zones II and III), for soil type *C*. Behaviour (i.e. force reduction) factors

q_y=2.50 and q_y=3.50 were adopted for Zones II and III, respectively, i.e. the bridge was designed as a ductile structure (plastic hinges expected to form in the piers). The lower q in the case of Zone II was due to the fact that the smaller column dimensions used in this case did not satisfy P-Δ requirements (θ_Δ) unless the 1st order moment (M^I) was increased through a lower q-value.

As specified in the Code, for prestressed members designed to remain elastic during the seismic event (i.e. the deck), the uncracked stiffness was used, whereas for the piers, wherein development of plastic hinging is expected under the design earthquake, the secant stiffness at yield is adopted, based on the maximum expected axial load. For the piers, the reduced stiffness was EI_{eff}=0.43EI_g and EI_{eff}=0.37EI_g, for Zone II and III designs, respectively. Linear static (rather than dynamic) analysis was used, to avoid introducing discrepancies between DDBD and FBD that are due to the type of analysis used; it is noted, though, that in Europe response spectrum analysis is typically used by bridge designers (even when this is not mandatory in the Code). Furthermore, the material safety factors used for determining member reinforcement were exactly the same in both DBD and FBD.

4.3 Evaluation of different designs

Design according to the current code provisions was applied mainly with a view to comparing the design base shear (V_B) and the required reinforcement ratio (ρ_{req}) to the ones resulting from the proposed design procedure. The main results are reported in Table 1, where pier displacement ductility (μ_Δ), member shear forces (V_i), equivalent cantilever lengths ($H_{0,i}$) and the percentage x of the total shear carried by the abutments are also shown. It is noted here that the displacement-based approach provides (among others) the ductility level for each pier (which is practically the same here, due to the symmetry of the bridge, but can be quite different in other configurations), while in the force-based approach, ductility requirements only enter the picture through the constant force reduction factor (2.50 and 3.50 for Seismic Zones II and III). Based on the equal displacement approximation and assuming no overstrength (which is a conservative assumption, as shown by Kappos et al. 2010) these factors can be assumed to be the ductility demand for all columns, as shown in the table under 'FBD'.

As shown in Table 1, in the case of Seismic Zone II design, the required design base shear is practically equal for the two different design approaches. On the other hand, in the high seismic hazard Zone III, the required base shear is 58% higher in the DDBD procedure (for the economy

of tables and figures in the case study we refer to 'DBD' values, meaning that all of them were derived using the DDBD method proposed herein). The discrepancy between the design base shears can be attributed to the different design 'philosophy' of each method; DDBD models the hysteretic response with the equivalent elastic secant stiffness to the maximum response in conjunction with an elastic displacement spectrum for the appropriate equivalent viscous damping (thus, the elastic response spectrum is multiplied with a damping modifier $R(\xi)\leq 1$), whereas FBD adopts the secant stiffness at yield and a 5%-damped elastic acceleration spectrum reduced through the behaviour factor q (multiplier equal to 1/q). Assuming that V_B can be approximately obtained from Equation 26 and given that M_{sys} is practically equal in the two design procedures (due to the fact that the first mode dominates the seismic response), the discrepancy between the design base shears can be illustrated in terms of acceleration spectra as shown in Figure 7 (in the case of DDBD the displacement response spectrum was converted to the corresponding acceleration response spectrum).

$$V_B = M_{SYS} \cdot S_a\left(T_{eff}\right) \tag{26}$$

Table 1. Key results from displacement-based design (DBD) and force-based design (FBD) of the bridge

Case	Member	V_B (kN)		x (%)		V_i (kN)		μ_Δ		q		R_ξ	1/q	H_o (m)		ρ_{req} (%)	
		DBD	FBD	DBD	FBD	DBD	FBD	DBD	FBD	DBD	FBD	DBD	FBD	DBD	FBD	DBD	FBD
Zone II (D=1.30 m)	Abt.1	2671.2	2688.1	30.0	12.9	399.1	173.7										
	Pier 2					933.6	1168.7	2.87	2.50	0.74	0.40			5.09	6.72	1.35	3.07
	Pier 3					936.0	1171.8	2.88	2.50					5.09	6.71	1.35	3.08
	Abt.4					402.6	174.0										
Zone III (D=1.70 m)	Abt.1	5590.9	3546.5	14.0	7.1	380.9	121.9										
	Pier 2					2383.7	1617.4	3.01	3.50	0.73	0.29			6.71	7.82	2.33	1.84
	Pier 3					2426.3	1676.9	3.07	3.50					6.71	7.78	2.35	1.93
	Abt.4					401.0	130.3										

In the case of Zone II, the required steel ratio for the bridge designed using the force-based procedure is approximately 2.3 times the displacement-based one, despite the fact that V_B was almost the same in the two methods. This result can be attributed to the fact that in the FBD the bridge attracts proportionally more shear force in its piers than the displacement-based one, since analysis is based on secant stiffness at yield rather than at peak response. In addition, higher values of pier stiffnesses (i.e. secant stiffness at yield) contribute to higher values of equivalent cantilever lengths (the pier tends to behave like a simple cantilever) and hence to increased longitudinal steel ratios at the base of the piers, as shown in Table 1. In this context, the similar

longitudinal steel ratios found in the case of Zone III result from the significantly higher base shear computed in the DBD procedure, when compared to the FBD one, as previously described.

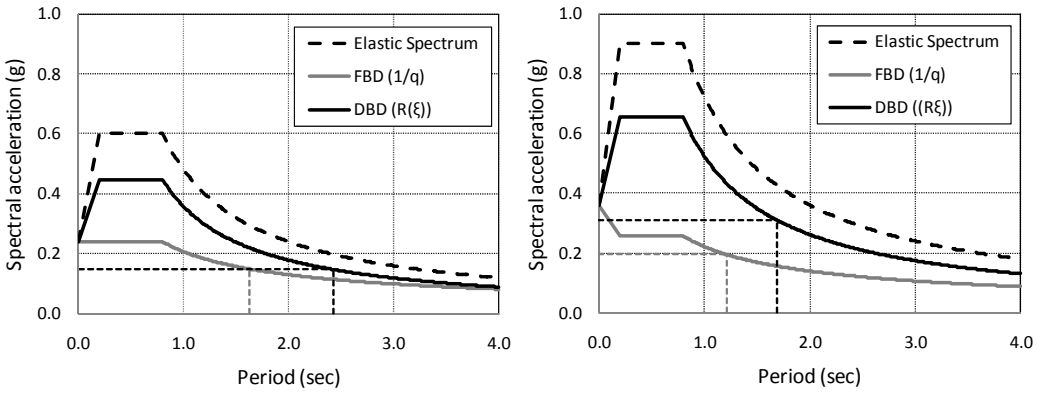

Figure 7. Spectral acceleration (corresponding to T_{eff}) definition based on the FBD and DBD design response spectra: Zone II (a_g = 0.36g) (left), and Zone III (a_g = 0.36g) (right)

5 Assessment of seismic performance through non-linear response history analysis

Assessment of the bridge designed for the two seismic zones according to DBD and FBD procedures was carried out in order to verify the accuracy of these methods in terms of meeting the target-displacement profile, and hence the target damage levels. Furthermore, the reliability of the design method was verified by comparing the pier design displacements and design ductility level with the displacement ductility demand obtained from inelastic dynamic analysis. Analyses were conducted with the program SAP2000 (CSI 2007) using the Takeda hysteretic model for the rotational spring elements, used for modelling the inelastically responding piers. Moment-rotation (M-θ) relationship was used with input parameters defined from fibre analysis performed for each critical pier section utilizing the computer program RCCOLA-90 (Kappos 1996). Elastomeric bearings were modelled using 'link' elements with 10% damping.

For each design case (Zone II or III), analysis was performed using one suite of seven real accelerograms from Greece, Turkey, and the US (California), and one suite of seven artificial records, generated with the computer program SIMQKE (Vanmarcke 1976) to fit the design spectra of Figures 2 and 6. The natural accelerograms have been selected and scaled to match the design spectra, in the period range between 0.2T_1 and 1.5T_1 sec, where T_1 is the value of the predominant (initial) period of the bridge designed for seismic Zones II and III, according to the

procedure prescribed in EC8-Part 2 (CEN 2005), modified with regard to the amount the ordinates of the elastic spectrum are exceeded within the critical range of periods, i.e. 0 instead of 30%, since deterministic assessment is sought (as opposed to design of the structure).

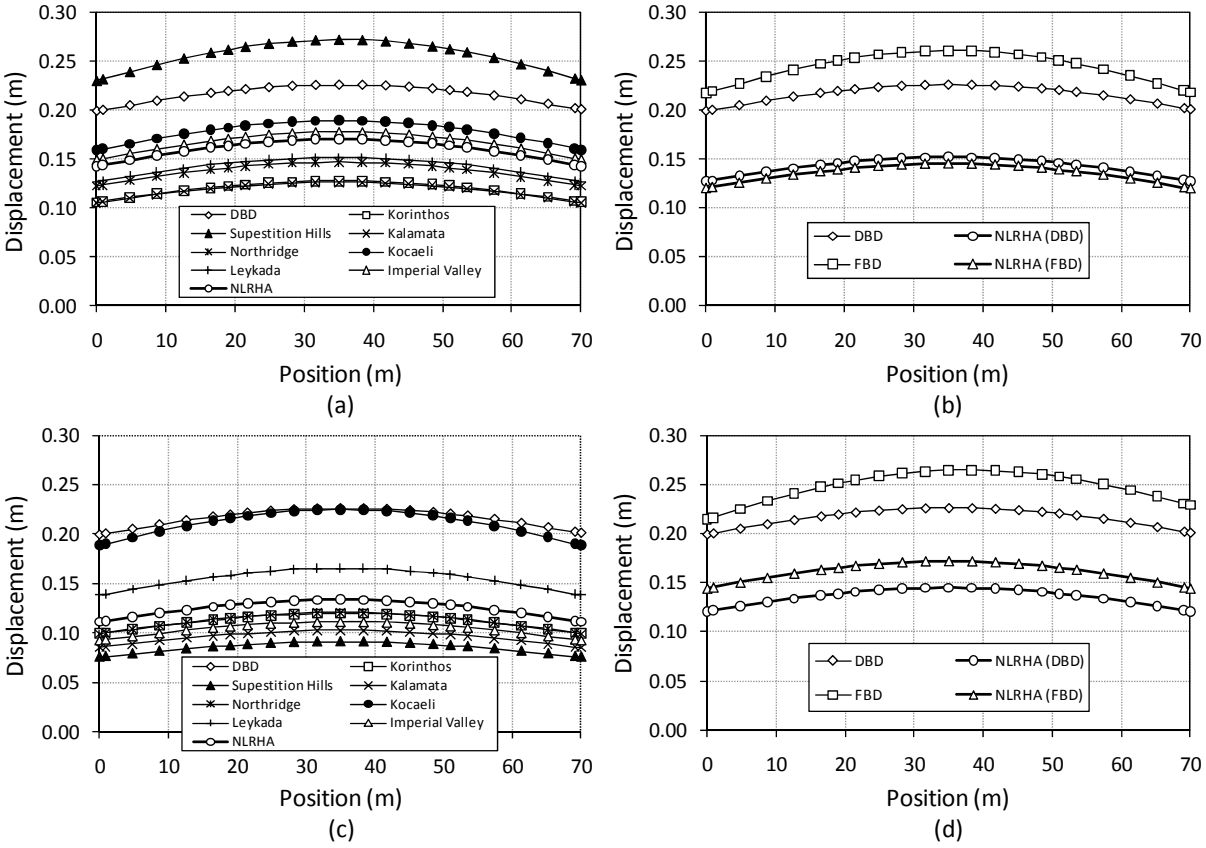

Figure 8. Comparison of deck transverse displacements obtained from DBD, FBD and nonlinear response-history analysis (NLRHA): (a) Seismic Zone II design - Suite of real accelerograms, (b) Seismic Zone II design - Suite of artificial accelerograms, (c) Seismic Zone III design - Suite of real accelerograms, (d) Seismic Zone III design - Suite of artificial accelerograms.

Shown in Figures 8a and 8c are deck transverse maximum displacements from response-history analysis (using natural records) juxtaposed to the design target profile obtained from DBD. Note that the target profile matches the analysis results reasonably well and is generally conservative with respect to amplitude (only one record resulted in displacements larger than the design ones, in the case of Zone II design, Figure 8a). This conservatism is primarily attributed to the overstrength of the pier critical sections, attributed to the use of mean values for material properties and consideration of strain-hardening of steel reinforcement. Since the overall deformed shape agrees well with that from response-history analysis, it is concluded that the

effective mode shape method was able to adequately capture the displacement pattern. Similar conclusions are drawn from Figures 8b and 8c (analyses for artificial records, where design displacements obtained from FBD and the corresponding NLRHA results (mean deck displacements derived for 7 records) are shown, in addition to target profiles and NLRHA results for DBD. In general, the shape of design displacement profile is closer to that derived from assessment (NLRHA) in the case of DBD, while for both designs (FBD and DBD) actual displacement values are quite lower than the design ones.

Further comparisons were made, involving the pier shear force (V) vs. lateral displacement (Δ) curves, obtained from the FBD and DBD method, and from NLRHA. Design V-Δ curves were drawn based on each method's assumptions, i.e. assuming that the post-elastic slope of the shear force vs. displacement response is zero, and computing yield displacement from Equation 4 (DBD) and from structural analysis for the design loads (FBD), whereas the maximum displacement corresponds to the pier's design target displacement. In the case of response-history analysis, the V-Δ relationship for a pier was obtained taking as yield displacement and yield shear force the displacement and shear values at the instant wherein the bending moment at the critical section first reaches the yield bending moment. The main goal of obtaining the V-Δ curves was to verify the reliability of the different designs in terms of ductility demand. The bridges were deemed as appropriately designed if the displacement ductility demand obtained from dynamic inelastic response-history analysis does not exceed the pier displacement ductility assumed in the DBD procedure (Step 5), or the q-factor used in the case of FBD. Figure 9 shows the aforementioned V-Δ curves for Pier 2 (M2 in Figure 3) for the two design cases in terms of the average of the calculated values in each nonlinear response-history analysis of the two sets of seismic excitations. In Figure 9b and 9d, V-Δ curves for the FBD case are also shown. The first remark regarding the curves in Figure 9 is that, as also shown in Fig. 8, design target displacement is 34% to 74% larger than the mean displacement demand (from NLRHA). As previously mentioned, this observation is attributed to pier overstrength, which results in higher pier stiffness than the value used in design. Similar trends can be observed with regard to pier displacement ductility, which is 24% to 73% larger than the ductility demand. This is expected, since yield displacement calculated from Equation 4 practically coincides with the one obtained by nonlinear response-history analysis, while the displacement demand is lower. The FBD designs are also found to be safe, in the sense that the required ductilities (μ= 1.5 and 2.2 for

Zones II and III, respectively) are substantially lower than the design ductility factor (μ≈q=2.5 and 3.5), for the previously mentioned reasons.

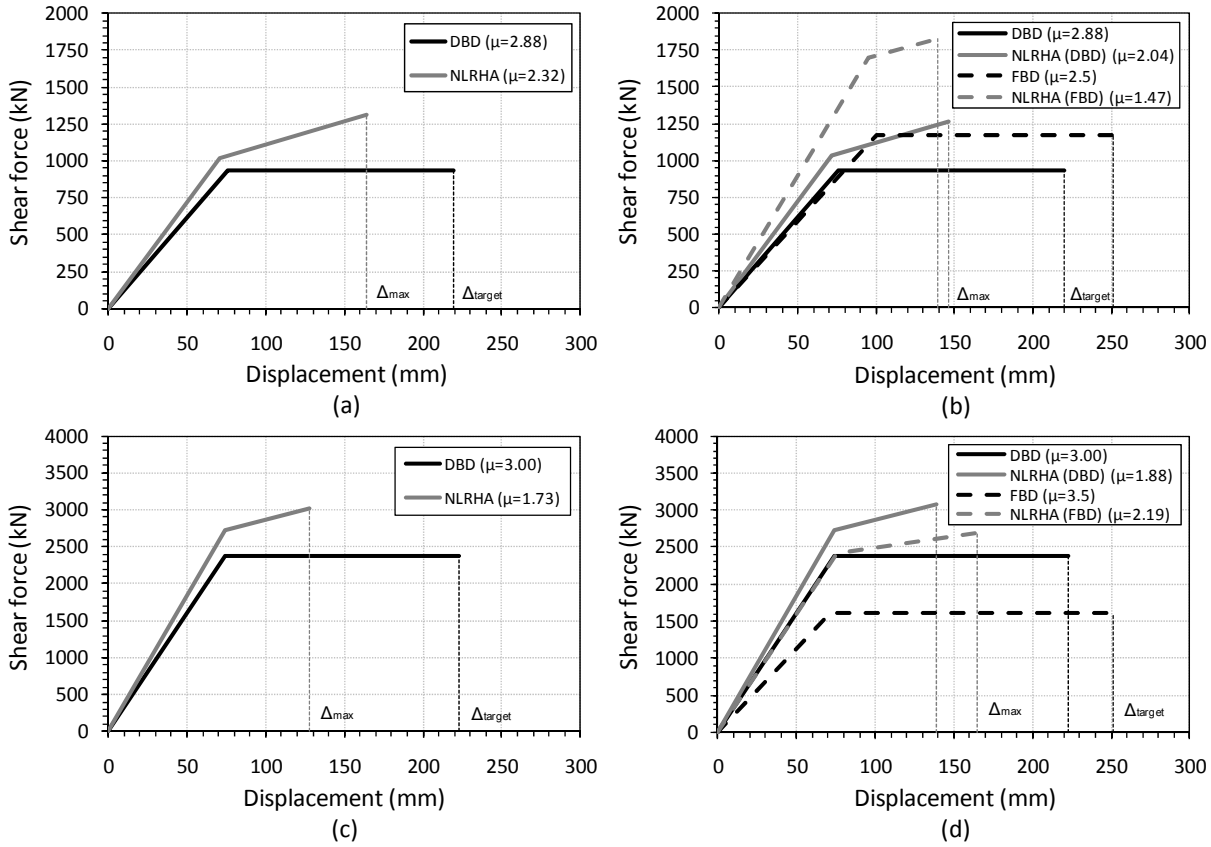

Figure 9. Comparison of Pier 2 peak shear force vs. displacement curves obtained from DBD, FBD and nonlinear response-history analysis (NLRHA): (a) Seismic Zone II design - Suite of real accelerograms, (b) Seismic Zone II design - Suite of artificial accelerograms, (c) Seismic Zone III design - Suite of real accelerograms, (d) Seismic Zone III design - Suite of artificial accelerograms.

6 Conclusions

An evaluation of the existing methodologies for direct displacement-based design of bridges was presented, and some improvements were suggested, with a view to making the method better suited for the final design of a fairly broad class of bridges, namely those supported by single-column piers. The feasibility and accuracy of the improved procedure were evaluated by applying it to an actual overpass bridge, designed to modern seismic practice; another case-study involving an overpass with different deck than that presented here can be found in Kappos et al (2011). The following conclusions (which have to be confirmed by additional case-studies involving different

bridge configurations) were reached by applying DBD and FBD, and assessing the resulting designs using NLRHA:

- DBD and FBD generally yield different values of the design base shear (V_B); in particular in the case of Zone II, the V_B obtained from DBD was found to be slightly lower than the one resulting from FBD, while in the case of Zone III it was found to be 58% higher. The discrepancy between the design base shears can be explained (see §5) on the basis of the different design 'philosophy' of each method.
- DBD provides a more rational base shear distribution among piers and abutments, compared to the FBD procedure. For instance, despite the fact that in the case of Zone II, V_B was almost the same in the two methods, the required steel ratio for the bridge designed using the FBD procedure was approximately 2.3 times the DBD one, due to the fact that in FBD the bridge attracted proportionally more shear force in its piers, and that in FBD secant stiffness at yield contributes to higher values of equivalent cantilever lengths.
- The improved DBD procedure was able to adequately capture the displacement pattern, closely matching the results of the more rigorous NLRHA. However, its feasibility was confirmed so far only in the case of bridges wherein the fundamental mode dominates the seismic response. Some preliminary results of the part of the present study addressing bridges with higher mode effects can be found in Kappos et al. (2011).
- The proposed version of DBD was found to lead to a 'safe' design on the grounds that pier displacements and displacement ductility demands obtained from NLRHA did not exceed the target values used in DBD. Moreover, the matching of yield displacements estimated using the proposed design procedure with those from the NLRHA indicates that the equivalent cantilever length estimated in the proposed DBD method was able to properly capture the degree of fixity at the top of the piers.

The extensions and/or modifications of the DBD proposed herein, with a view to making it applicable to final (as opposed to preliminary) design of actual bridges, as a rule require a substantial number of iterations, i.e. they increase the complexity of the method and the computational effort involved. Therefore a full implementation of the proposed procedure in a software package would significantly increase its usefulness in practical design. On the other hand, this increased effort is compensated by the increased reliability of the results, which

provides grounds for adopting the DDBD as a practical design procedure without mandatory verification of the final results through nonlinear analysis as required by current codes.

Acknowledgements

The contribution of Asst. Prof. A. Sextos (from the Department of Civil Engineering of the Aristotle University of Thessaloniki) to the computational aspects of this work is gratefully acknowledged.

References

Adhikari, G., Petrini, L., Calvi, G. M., 2010. Application of direct displacement based design to long-span bridges, *Bull Earthquake Engineering,* **8** (4), 897–919.

American Association of State Highway and Transportation Officials (AASHTO) 2009. *Guide Specifications for LRFD Seismic Bridge Design*, Washington, D.C.

American Society of Civil Engineers (ASCE), 2006. *Minimum Design Loads for Buildings and other Structures, ASCE Standard ASCE/SEI 7-05*, Reston, VA.

Bardakis, V. G., and Fardis, M. N., 2008. Displacement-based seismic design of concrete bridges, in *Proceedings, 14th World Conference on Earthquake Engineering*, Beijing, China, Paper No. 05-02-0017.

Calvi, G. M., and Kingsley, G. R., 1995. Displacement-based seismic design of multi-degree-of-freedom bridge structures, *Earthquake Engineering & Structural Dynamics*, **24** (9), 1247-1266.

CEN (Comité Europeen de Normalization) 2005. *Eurocode 8, design of structures for earthquake resistance—part 2: bridges*, CEN, Brussels.

Christopoulos, C., and Filiatraut A., 2006. *Principles of Passive Supplemental Damping and Seismic Isolation*, 1st edition, IUSS Press, Pavia, Italy, 480 pp.

CSI, (2007). SAP200: Three Dimensional Static and Dynamic Finite Element Analysis and Design of Structures, Computers and Structures Inc., Berkeley, CA.

Dwairi, H., and Kowalsky, M. J., 2006. Implementation of inelastic displacement patterns in direct displacement-based design of continuous bridge structures, *Earthquake Spectra*, **22** (3), 631-662.

Kappos, A. J., 1996. RCCOLA-90: A Microcomputer Program for the Analysis of the Inelastic Response of Reinforced Concrete Sections, Department of Civil Engineering, Aristotle University of Thessaloniki, Greece.

Kappos, A. J., 2010. *Current Trends in the Seismic Design and Assessment of Buildings*, Ch. 11 in *Earthquake Engineering in Europe, Geotechnical, Geological, and Earthquake Engineering*, Garevski, M., Ansal, A., (Eds.), Springer, 568 pp.

Kappos, A. J., and Sextos, A. G., 2009. Seismic assessment of bridges accounting for nonlinear material and soil response, and varying boundary conditions, in *Proceedings, Coupled Site and Soil-Structure Interaction Effects with Application to Seismic Risk Mitigation*, NATO SfP&S Series-C, Springer, pp. 195-208.

Kappos, A.J., Gkatzogias, K.I., Gidaris, I., 2011. An improved displacement-based seismic design methodology for bridges accounting for higher mode effects. COMPDYN'11 (Computational Methods in Structural Dynamics and Earthquake Engineering, Corfu, Greece, May 2011), paper no. 256.

Kappos, A., Paraskeva, T., and Moschonas, I., 2010. What are the actual q-factors of Egnatia bridges? *Aseismic design and construction in Egnatia Odos*, Hellenic Society for Earthquake Engineering, Thessaloniki.

Katsaras, C. P., Panagiotakos, T. B., and Kolias, B., 2009. Effect of torsional stiffness of prestressed concrete box girders and uplift of abutment bearings on seismic performance of bridges, *Bulletin of Earthquake Engineering*, **7** (2), 363-375.

Kowalsky, M. J., 2000. Deformation limit states for circular reinforced concrete bridge columns, *Journal of Structural Engineering*, **126** (8), 869-878.

Kowalsky, M. J., 2002. A displacement-based approach for the seismic design of continuous concrete bridges, *Earthquake Engineering & Structural Dynamics*, **31** (3), 719-747.

Kowalsky, M. J., Priestley, M. J. N., and MacRae, G. A., 1995. Displacement-based design of RC bridge columns in seismic regions, *Earthquake Engineering & Structural Dynamics*, **24** (12), 1623-1643.

Mitoulis, S. A. and Tegos, I. A., 2010. An external restraining system for the seismic retrofit of existing bridges. 9th US National & 10th Canadian Conference on Earthquake Engineering, Toronto 25-29 July, paper no. 70.

Paraskeva, T., and Kappos, A. J., 2010. Further development of a multimodal pushover analysis procedure for seismic assessment of bridges, *Earthquake Engineering & Structural Dynamics*, **39** (2), 211 – 222.

Priestley, M. J. N., Calvi, G. M., and Kowalsky M. J., 2007. Displacement-based seismic design of structures, 1st edition, IUSS Press, Pavia, Italy, 720 pp.

SEAOC Ad Hoc Committee, 1999. *Tentative Guidelines for Performance-based Seismic Engineering*, App. I of: *Recommended lateral force requirements and Commentary*, SEAOC, Sacramento, CA.

Shibata, A., and Sozen, M., 1976. Substitute structure method for seismic design in reinforced concrete, *J. Struct. Div.*, **102** (ST1), 1–18.

Suarez V.A. and Kowalsky, M.J., 2010. Direct Displacement-Based Design as an Alternative Method for Seismic Design of Bridges. ACI SP-271: *Structural Concrete in Performance-Based Seismic Design of Bridges*, pp. 63-77.

Vanmarcke, E. H., 1976. SIMQKE: A Program for Artificial Motion Generation, Civil Engineering Department, Massachusetts Institute of Technology.

APPENDIX A: Detailed design using the DDBD approach

For **Zone II** (a_g=0.24g) a 1.30 m column diameter was selected for both piers, and as a first estimate, based on the assumption of inelastic response of the piers, their secant stiffness was taken to be equal to 10% of the uncracked stiffness (K_g). The effective horizontal stiffness of the elastomeric bearings, assigned for shear strain $\gamma \leq 2.0$, was equal to 1010 kN/m, calculated on the basis of the mechanical and geometrical properties of the selected bearings (Christopoulos & Filiatraut 2006). A secant torsional stiffness equal to 20% of the superstructure's uncracked torsional stiffness was used as an appropriate value for the torsional stiffness of prestressed concrete decks subsequent to concrete cracking (Katsaras et al. 2009).

Equivalent cantilever length (H_0): As a first estimate it is assumed that the equivalent cantilever length (H_0) is equal to the total length of the pier H=9.48 m, measured to the superstructure's mass centroid. Consequently, the initial ratio n of the equivalent cantilever length to the total length is equal to 1.0; this will be revised after the first iteration.

Yield displacement: The yield curvature is estimated as (Priestley et al. 2007):

$$\varphi_y = 2.25 \cdot \frac{\varepsilon_y}{D} = 2.25 \cdot \frac{0.0025}{1.30} = 0.0043 / \text{m}$$

For the purposes of yield displacement calculation, a strain penetration length L_{sp}=0.022·f_y·d_b=0.022·500·0.025 is added to the column height, where d_b is the longitudinal reinforcement diameter (25mm). The yield displacement is then:

$$\Delta_y = n \cdot \varphi_y \cdot \frac{(H + L_{sp})^2}{3} = 1 \cdot 0.0043 \cdot \frac{(9.477 + 0.275)^2}{3} = 0.137 \text{ m}$$

Limit state displacement capacities: The limit state displacement capacities for the piers are calculated using the criterion of 3% drift ratio:

$$\Delta_{d,pier} = 0.03 \cdot 9.477 = 0.284 \text{ m}$$

Moreover, an upper limit in pier displacement ductilities of μ_u=6 was adopted. Considering an allowable shear strain γ_u=2.0 for the elastomeric bearings at the abutments, their limit state displacement capacity is:

$$\Delta_{d,bearing} = \gamma_u \cdot t_e = 2.00 \cdot 0.100 = 0.200 \text{ m}$$

where t_e is the total thickness of the elastomer. The steps of the proposed design procedure are then applied as follows:

Step 1 - Estimation of the displacement pattern of the bridge: Applying the effective mode shape method (Kowalsky 2002), outlined in the third section of the paper, the following normalized displacement pattern (δ_i) was obtained: δ_1=0.898, δ_2=0.997, δ_3=1.000 and δ_4=0.902 m, wherein points 1 and 4 refer to the abutments (A1 and A2 in Figure 3) and 2, 3 to the two piers (M1, M2 in Figure 3). Note that displacements at the abutments are about 90% those at the piers, a clear indication that the superstructure is relatively rigid compared to the substructure, which is anticipated in a bridge with a prestressed concrete deck, relatively short spans and relatively short piers.

Step 2 - Estimation of the fraction of the total seismic force carried by the abutments: A value of x=0.30 is selected (Dwairi & Kowalsky 2006) as an initial guess for the fraction of lateral force transmitted to the abutments.

Step 3 - Definition of the critical target displacement profile: The critical target displacement profile (Δ_i) is obtained by scaling the displacement pattern (δ_i) to the limit state displacement capacity of the critical abutment 4, according to Equation 11. The following profile is calculated: Δ =0.199, Δ_2=0.221, Δ_3=0.222 and Δ_4=0.200 m.

Step 4 - Determination of the equivalent SDOF system: In order to determine the equivalent SDOF system displacement from Equation 12, the masses for each abutment and pier must first be defined. The masses are assumed to include the tributary superstructure mass and 1/3 of the mass of each pier. The masses at the top of the piers are: m_2=m_3=726.44 tn, while at the abutments m_1=m_4=199.34 tn. Hence, the system displacement is:

$$\Delta_{sys} = \frac{199.34 \cdot (0.199^2 + 0.200^2) + 726.44 \cdot (0.221^2 + 0.222^2)}{199.34 \cdot (0.199 + 0.200) + 726.44 \cdot (0.221 + 0.222)} = 0.217 \text{ m}$$

The equivalent SDOF system mass is calculated from Equation 13:

$$M_{sys} = \frac{1}{0.217} \cdot [199.34 \cdot (0.199 + 0.200) + 726.44 \cdot (0.221 + 0.222)] = 1848.4 \text{ tn}$$

Step 5 - Determination of the pier displacement ductilities and equivalent viscous damping ratios: The displacement ductilities for the piers are: $\mu_{\Delta,2}$=0.221/0.137=1.61 and $\mu_{\Delta,3}$=0.222/0.137=1.62, (design criterion iv is valid). Utilizing Equation 14 and adding 5% viscous damping, the following equivalent damping values for the piers are calculated:

$$\xi_2 = 5 + 44.4 \cdot \left(\frac{1.61 - 1}{1.61 \cdot \pi} \right) = 10.36\%$$

$$\xi_3 = 5 + 44.4 \cdot \left(\frac{1.62 - 1}{1.62 \cdot \pi} \right) = 10.39\%$$

As mentioned in the paper, the elastomeric bearings at the abutments have equivalent viscous damping equal to 10%, i.e. very close to that of the piers.

Step 6 - Determination of the base shear distribution among different bents: From Equations 16 and 17 the shear force carried by each individual bent is given by:

$$V_2 = V_3 = (1 - 0.3) \cdot \left(\frac{1/9.477}{1/9.477 + 1/9.477} \right) \cdot V_B = 0.35 \cdot V_B$$

$$V_1 = V_4 = 0.15 \cdot V_B$$

Step 7 - Determination of the equivalent system damping: The equivalent system damping is calculated from Equation 18 as follows:

$$\xi_{sys} = \frac{0.15 \cdot (0.199 + 0.200) \cdot 10.0 + 0.35 \cdot 0.221 \cdot 10.36 + 0.35 \cdot 0.222 \cdot 10.39}{0.15 \cdot (0.199 + 0.200) + 0.35 \cdot 0.221 + 0.35 \cdot 0.222} = 10.27\%$$

Step 8 - Determination of the effective period, stiffness and design base shear of the equivalent SDOF system: According to Eurocode 8, the spectral displacement reduction factor for the calculated system damping is $R(\xi)=(10/(5+10.27))^{0.5}$=0.809. Reducing the 5% displacement design spectra shown in Figure 6 and entering with system displacement of 0.217 m

(from Step 4), the effective period of the equivalent SDOF system is found to be T_{eff}=2.25≤T_D=4.0 sec (design criterion i is valid). The effective stiffness is obtained from Equation 19:

$$K_{eff} = 4 \cdot \pi^2 \cdot \frac{1848.4}{2.25^2} = 14418 \text{ kN/m}$$

Therefore, the seismic base shear is equal to V_B=14418·0.217=3129.1 kN.

Once the target displacement profile has been established, the base shear and the elastomeric bearings' effective horizontal stiffness are known, and the fraction of the seismic force, *x*, which is carried by the bearings at the abutments, can be recalculated, given the assumption that their force-displacement relationship is linear. Thus, the shear forces carried by the two bearings of each abutment are V_1=2·1010·0.199=401.98 kN and V_2=2·1010·0.200=404.00 kN, and the ratio *x* is:

$$x = \frac{401.98 + 404.00}{3129.1} = 0.258$$

Note that the revised ratio *x* is slightly less than the assumed value (30%). Although this difference is not expected to change significantly the properties of the equivalent SDOF system, these quantities are recalculated as shown below:

$$\xi_{sys} = 10.29\%;\ T_{eff} = 2.25 \text{ sec};\ K_{eff} = 14403.4 \text{ kN/m};\ V_B = 3126.02 \text{ kN}$$

Step 9 - Verification of effective pier stiffnesses: Utilizing the revised value of the ratio *x*, the base shear is distributed as follows:

$$V_1 = x \cdot \frac{\Delta_1}{\Delta_1 + \Delta_4} \cdot V_B = 0.258 \cdot \frac{0.199}{0.199 + 0.200} \cdot 3126.02 = 401.81 \text{ kN}$$

$$V_4 = x \cdot \frac{\Delta_4}{\Delta_1 + \Delta_4} \cdot V_B = 0.258 \cdot \frac{0.200}{0.199 + 0.200} \cdot 3126.02 = 403.60 \text{ kN}$$

$$V_2 = V_3 = (1 - 0.258) \cdot \frac{1/9.477}{1/9.477 + 1/9.477} \cdot 3126.02 = 1160.31 \text{ kN}$$

Now the preliminary assumption that all piers have effective stiffnesses equal to 10% of the uncracked stiffness is checked. The effective stiffnesses are calculated according to Equation 21 as follows:

$$K_2 = 1160.31/0.221 = 5248.9 \text{ kN/m } (33.99\% \text{ of } K_g)$$
$$K_3 = 1160.31/0.222 = 5234.7 \text{ kN/m } (33.90\% \text{ of } K_g)$$

Because of the difference between the assumed effective stiffnesses and the calculated ones, a second iteration involving Steps 1 to 9 is needed. The second iteration results are shown in Table A.1; however, there is still some difference between assumed and calculated stiffness values. One additional iteration was carried out until the effective stiffnesses stabilized.

Table A.1. Summary of design iterations (equivalent cantilever length: H_0 = 9.477 m)

Step	Item	Abutment 1	Pier 2	Pier 3	Abutment 4
	2nd ITERATION				
Step 1	**Displacement pattern, δ_i**	0.859	0.994	1.000	0.869
Step 2	**Ratio of the seismic force carried by the abutments, x**		0.269		
Step 3	**Target displacement profile, Δ_i (m)**	0.198	0.229	0.230	0.200
Step 4	**System displacement, Δ_{sys} (m)**		0.223		
	System mass, M_{sys} (ton)		1845.660		
Step 5	**Displacement ductility, $\mu_{\Delta,i}$**		1.67	1.68	
	Equivalent damping, $\xi_{eq,i}$ (%)	10.00	10.66	10.71	10.00
Step 6	**Shear force distribution, V_i / V_B**	0.134	0.365	0.365	0.135
Step 7	**System damping, ξ_{sys} (%)**		10.52		
	System effective period, T_{eff} (sec)		2.335		
Step 8	**System effective stiffness, K_{eff} (kN/m)**		13362.46		
	Design base shear, V_B (kN)		2986.33		
	Member shear force, V_i (kN)	399.35	1091.39	1091.39	404.19
Step 9	**Member effective stiffness, K_i (kN/m)**	2020.00	4772.93	4744.29	2020.00
	Ratio, K_i / $K_{g,i}$ (%)		30.91	30.72	
	3rd ITERATION				
Step 1	**Displacement pattern, δ_i**	0.855	0.990	1.000	0.874
Step 2	**Ratio of the seismic force carried by the abutments, x**		0.265		
Step 3	**Target displacement profile, Δ_i (m)**	0.196	0.227	0.229	0.200
Step 4	**System displacement, Δ_{sys} (m)**		0.222		
	System mass, M_{sys} (ton)		1845.780		
Step 5	**Displacement ductility, $\mu_{\Delta,i}$**		1.65	1.67	
	Equivalent damping, $\xi_{eq,i}$ (%)	10.00	10.58	10.66	10.00
Step 6	**Shear force distribution, V_i / V_B**	0.131	0.367	0.367	0.134
Step 7	**System damping, ξ_{sys} (%)**		10.47		
	System effective period, T_{eff} (sec)		2.317		
Step 8	**System effective stiffness, K_{eff} (kN/m)**		13573.09		
	Design base shear, V_B (kN)		3013.92		
	Member shear force, V_i (kN)	395.39	1107.30	1107.30	403.94
Step 9	**Member effective stiffness, K_i (kN/m)**	2020.00	4884.60	4837.22	2020.00
	Ratio, K_i / $K_{g,i}$ (%)		31.63	31.33	
	CONVERGENCE ACHIEVED				

Step 10 - Distribution of design base shear force to inertia mass locations: Utilizing Equation 22, the base shear force is distributed to each of the four inertia mass locations. The inertia forces are:

$$F_1 = 3013.92 X \frac{199.34 X 0.196}{199.34 X 0.196 + 726.44 X 0.227 + 726.44 X 0.229 + 199.34 X 0.200} = 286.96 \text{ kN}$$

$$F_2 = 3013.92 X \frac{726.44 X 0.227}{199.34 X 0.196 + 726.44 X 0.227 + 726.44 X 0.229 + 199.34 X 0.200} = 1210.97 \text{ kN}$$

$$F_3 = 3013.92 X \frac{726.44 X 0.229}{199.34 X 0.196 + 726.44 X 0.227 + 726.44 X 0.229 + 199.34 X 0.200} = 1222.83 \text{ kN}$$

$$F_4 = 3013.92 X \frac{199.34 X 0.200}{199.34 X 0.196 + 726.44 X 0.227 + 726.44 X 0.229 + 199.34 X 0.200} = 293.17 \text{ kN}$$

Step 11 – Structural analysis: The structure is then analyzed for the previous inertia forces (Step 10), utilizing the effective stiffnesses from the third iteration (see Table A.1) as an initial guess. To reduce the effort required for updating member stiffnesses, the software used should be capable of defining member rigidities (EI_{eff}) as a fraction of the gross rigidity (EI_g).

Step 12 – Verification of the target-displacement profile: The displacement of the critical member (abutment 4) is compared with the corresponding assumed target displacement. Because of the observed difference the pier stiffness is changed accordingly and the analysis is repeated until convergence is achieved. The results from structural analysis are shown in Table A.2.

Table A.2. Summary of structural analysis (equivalent cantilever length $H_0 = 9.477$ m)

Item	Abutment 1	Pier 2	Pier 3	Abutment 4
1st ITERATION				
Assumed ratio of the seismic force carried by the abutments, x		0.265		
Assumed target displacement profile, Δ_i (m)	0.196	0.227	0.229	0.200
Assumed member shear force, V_i (kN)	395.39	1107.30	1107.30	403.94
Assigned pier effective stiffness (% K_g)		31.63	31.33	
Analysis displacement profile (m)	0.115	0.133	0.134	0.118
Analysis member shear force (kN)	229.20	1268.50	1280.90	235.40
Analysis ratio of the seismic force carried by the abutments, x		0.154		
2nd ITERATION				
Revised pier effective stiffness (% K_g)		11.10	11.10	
Analysis displacement profile (m)	0.197	0.220	0.222	0.201
Analysis member shear force (kN)	394.70	1103.10	1114.56	401.54
Analysis ratio of the seismic force carried by the abutments, x		0.264		
CONVERGENCE ACHIEVED				

Step 13 – Verification of equivalent cantilever length: Once the displacement profile obtained from structural analysis converges to the assumed target – displacement profile, the equivalent cantilever length obtained from the analysis ($H_{0,analysis}$=5.27 m) is compared with the initial value which was assumed at the beginning of the procedure (H_0=9.48 m). Note that the analysis equivalent cantilever length differs significantly from the assumed one. Therefore, additional iterations involving Steps 1 to 13 are conducted. In these new iterations the revised equivalent cantilever length is utilized to calculate the new yield displacements from Equation 4. The values obtained from the previous step serve as initial guesses of the effective stiffnesses and ratio *x* (11.10% K_g and 26.4%, respectively). Two iterations within Steps 1 to 9 were needed until the effective stiffnesses stabilized, while two structural analyses are performed until convergence of target displacement is achieved (Steps 11 to 12). Only the results from the final iteration are presented in Table A.3.

Since displacement profile, member shear forces and equivalent cantilever length did not change significantly with respect to the assumed ones, the iterative part of the design procedure (Steps 1 to 13) is concluded.

Step 14 - Verification of P-Δ effects: The critical pier for the verification of P-Δ effects is pier 3. The displacement and the axial load at the point of contraflexure and the base moment of pier 3 obtained from the structural analysis are the following:

$$P = 7322.6 \text{ kN};\ \Delta = 0.122 \text{ m};\ M = 4758.98 \text{ kNm}$$

Utilizing these values, the stability index is calculated from Equation 23

$$q_D = \frac{7322.6 \times 0.122}{4758.98} = 0.187 < 0.20$$

As this exceeds 0.10 and is less than 0.20, the design moment at the pier's base is amplified in accordance to Equation 24:

$$M_{design} = 4758.98 + 0.5 \times 7322.6 \times 0.122 = 5204.00 \text{kNm}$$

Table A.3. Final design iteration

Step	Item	Abutment 1	Pier 2	Pier 3	Abutment 4
-	Assumed equivalent cantilever length, H_0 (m)		5.27	5.27	
-	Yield displacements, $\Delta_{y,i}$ (m)		0.0763	0.0763	
-	Assigned pier effective stiffness (% K_g)		11.10	11.10	
-	Assumed ratio of the seismic force carried by the abutments, x			0.264	
	REVISED TARGET - DISPLACEMENT PROFILE AFTER 1ST ITERATION OF STEPS 1 TO 9				
Step 1	Displacement pattern, δ_i	0.9037	0.9963	1.0000	0.9101
Step 2	Ratio of the seismic force carried by the abutments, x			0.301	
Step 3	Target displacement profile, Δ_i (m)	0.1986	0.2189	0.2198	0.2000
Step 4	System displacement, Δ_{sys} (m)			0.215	
	System mass, M_{sys} (ton)			1848.824	
Step 5	Displacement ductility, $\mu_{\Delta,i}$		2.87	2.88	
	Equivalent damping, $\xi_{eq,i}$ (%)	10.00	14.21	14.23	10.00
Step 6	Shear force distribution, V_i / V_B	0.150	0.350	0.350	0.151
Step 7	System damping, ξ_{sys} (%)			13.03	
	System effective period, T_{eff} (sec)			2.426	
Step 8	System effective stiffness, K_{eff} (kN/m)			12404.24	
	Design base shear, V_B (kN)			2671.24	
	Member shear force, V_i (kN)	400.44	933.76	933.76	403.28
Step 9	Member effective stiffness, K_i (kN/m)	2020.00	4264.84	4249.06	2020.00
	Ratio, K_i / $K_{g,i}$ (%)		8.54	8.51	
Step 10	Inertia forces, F_i (kN)	265.60	1067.10	1071.06	267.48
	RESULTS OF 2nd STRUCTURAL ANALYSIS				
	Revised member effective stiffness, Ki (kN/m)	2020.00	4253.26	4245.03	2020.00
Steps 11 - 12	Revised pier effective stiffness (% K_g)		8.60	8.57	
	Analysis displacement profile (m)	0.1992	0.2195	0.2205	0.2009
	Analysis member shear force (kN)	399.10	933.59	936.03	402.60
	Analysis ratio of the seismic force carried by the abutments, x			0.300	
	Analysis equivalent cantilever length (m)		5.09	5.09	
	Analysis pier base moment (kNm)		4749.80	4758.98	
	CONVERGENCE ACHIEVED				

Step 15 - Design of the MDOF structure: Finally the bridge is designed in accordance with capacity design principles in order to prevent any sort of brittle failure. The required longitudinal steel ratio for the piers is 1.35% (>1% which is the minimum required and hence design criterion ii is satisfied).

A summary of the results for the other case (Seismic **Zone III** design) is given in Table A.4.

Table A.4. Summary of design results for the Seismic Hazard Zone III design case

Item	Abutment 1	Pier 2	Pier 3	Abutment 4
Target displacement profile, Δ_i (m)	0.192	0.224	0.228	0.200
System displacement, Δ_{sys} (m)		0.220		
System mass, M_{sys} (ton)		1845.410		
Displacement ductility, $\mu_{\Delta,i}$		3.01	3.07	
System damping, ξ_{sys} (%)		13.93		
System effective period, T_{eff} (sec)		1.694		
System effective stiffness, K_{eff} (kN/m)		25394.60		
Design base shear, V_B (kN)		5590.92		
Member shear force, V_i (kN)	380.90	2383.70	2426.27	401.00
Ratio of the seismic force carried by the abutments, x		0.140		
Equivalent cantilever length, H_0 (m)		6.55	6.55	
Pier base moment (kNm)		15650.05	15820.00	
Required pier steel ratio (%)		2.33	2.35	